Assessment of Windkessel as a model of aortic input impedance

DANIEL BURKHOFF, JOE ALEXANDER, JR., AND JOCHEN SCHIPKE
Department of Biomedical Engineering, The Johns Hopkins Medical School, Baltimore, Maryland 21205

BURKHOFF, DANIEL, JOE ALEXANDER, JR., AND JOCHEN SCHIPKE. *Assessment of Windkessel as a model of aortic input impedance.* Am. J. Physiol. 255 (Heart Circ. Physiol. 24): H742–H753, 1988.—To facilitate the analysis of aortic-ventricular coupling, simplified models of aortic input properties have been developed, such as the three-element Windkessel. Even though the impedance spectrum of the Windkessel reproduces the gross features of the real aortic input impedance, it fails to reproduce many of its details. In the present study we assessed the physiological significance of the differences between real and Windkessel impedance. We measured aortic input impedance spectra from five anesthetized open-chest dogs under a wide range of conditions. For each experimentally determined spectrum we estimated the corresponding values of the best-fit Windkessel parameters. By computer simulation we imposed both the real and best-fit Windkessel impedances on a model left ventricle and assessed the differences in seven different coupling variables. The analysis indicated that the Windkessel model provides a reasonable representation of afterload for purposes of predicting stroke volume, stroke work, oxygen consumption, and systolic and diastolic aortic pressures. However, the Windkessel model significantly underestimates peak aortic flow, slightly underestimates mean arterial pressure, and, of course, does not provide realistic aortic pressure and flow waveforms.

aortic-ventricular coupling; impulse response; spectral analysis; cardiovascular simulation; stroke volume; stroke work; myocardial oxygen consumption; aortic pressure

THERE HAS BEEN long-standing interest in the elucidation of determinants of cardiovascular function by understanding the coupling between the left ventricle and its arterial afterload [see Yin (27) for a recent review]. Toward this end, much effort has been devoted to the discovery of independent quantitative characterizations of ventricular contractile properties and arterial pressure-flow relations. Ventricular properties are now commonly represented by pressure-volume-flow relationships in the time domain (5, 17, 20). To describe ventricular afterload, arterial properties have been most extensively studied in terms of aortic input impedance, which is a frequency domain analysis of the pulsatile arterial pressure-flow relationship measured form the aortic root (9, 12, 14). To analyze aortic-ventricular (A-V) coupling, such representations must be mathematically interfaced and the resulting equations solved by analytical or, more commonly, numerical methods. Although mathematical coupling of the time domain representation of ventricular function and the frequency domain representation of the afterload in the presence of the aortic valve (rendering the system nonlinear) is possible, it is also quite cumbersome (as will be shown below).

To facilitate the investigation of A-V coupling, simplified analog or hydraulic models, whose input impedances resemble those of the real arterial system, have been developed. With such models, the coupling equations take the form of differential equations that can be solved by simple numerical calculations. The model that has been most extensively used in studies of A-V coupling in recent years is the three-element Windkessel (6, 21, 25–27), which is depicted in Fig. 1. The three parameters of this model are the characteristic impedance (R_c), the peripheral arterial resistance (R_a), and the arterial compliance (C_a). Significant advances in the understanding of A-V coupling have been made under the assumption that this or closely related models reproduce the real aortic input impedance with sufficient accuracy. It is well known, however, that while the Windkessel model captures many of the gross features of the real impedance, it fails to reproduce many of its details (21, 25, 26). The physiological significance of the deviations of the Windkessel model behavior from reality have not been assessed. Thus the extent to which the understanding of A-V coupling gained through studies that employ the Windkessel assumption as it pertains to the more realistic situation is not known.

Therefore the purpose of the present study was to quantitatively assess the validity of the Windkessel model for the purpose of studying A-V coupling. To accomplish this we first determined aortic input impedance spectra from open-chest dogs by use of white noise analysis, as described previously (24). (From this point on, we will refer to these experimentally determined spectra as "real impedance spectra.") For each real impedance spectrum, we determined the parameter values of the Windkessel model that best fit the data. Finally, by computer simulation, we loaded a model left ventricle with both the real and best-fit Windkessel impedance spectra and assessed the differences through an evaluation of several coupling variables, including stroke volume, stroke work, total pressure-volume area [a correlate of myocardial oxygen consumption (19)], peak aortic flow, and systolic, diastolic, and mean arterial pressures. The interaction between the model ventricle and either the real aortic input impedance or the Windkessel impedance was accomplished by use of the time

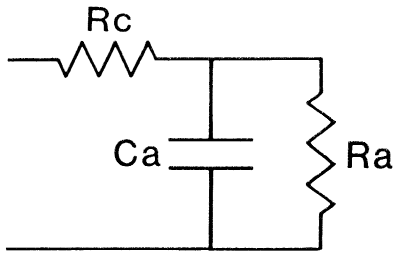

FIG. 1. Three-element Windkessel model. Three parameters are characteristic impedance (R_c), arterial resistance (R_a), and arterial compliance (C_a).

domain representation of the aortic input impedance called the "impulse response," which is obtained by taking the inverse Fourier transform of the impedance spectrum.

METHODS

Surgical procedures. Data were obtained from a total of five mongrel dogs of either sex that weighed on average 23 kg. Each dog was anesthetized with pentobarbital sodium (30 mg/kg iv), intubated, and respirated on room air supplemented with 95% O_2-5% CO_2 at a rate of 4–5 l/min. The thorax was opened via a median sternotomy in addition to a left lateral thoracotomy in the fourth intercostal space, the latter performed to allow easy access to the left atrium (to which a reservoir was connected, as described below). The pericardium was opened and used to make a cradle that supported the heart. The proximal aortic root was exposed by blunt dissection of the surrounding adipose and connective tissue. To measure aortic flow, a Transonic flow probe of either a 14- or 17-mm diameter (probe size best matching the aortic diameter) was positioned around the aortic root as proximal to the aortic valve as possible. The flowmeter (Transonic Systems, Ithaca, NY) measures volume flow directly, irrespective of vessel size and flow velocity profile; it also provides automatic zeroing and calibration capabilities (that have been confirmed in our lab). Acoustic coupling between the probe and aorta was made by commercially available acoustic jelly. The flowmeter introduces a fixed 8-ms delay that was corrected for in calculations of the impedance spectrum as described below. To measure aortic pressure at the site of the flow probe, a 7-F micromanometer tip Millar catheter was introduced into the left femoral artery and advanced to a position just distal to the flow probe as follows. With the catheter sitting within its core, the flow probe failed to operate properly, as manifested by noise on the flow signal and loss of the zero base line. The catheter was initially advanced within the field of the flow probe and then slowly withdrawn until a clean signal was obtained with normal zero during diastole. Catheter positioning by this method was examined at the end of several experiments by direct inspection after dissection of the aortic wall. We found that the catheter tip was between 0.3 and 0.8 cm from the center of the flow probe.

The left atrium was cannulated with a line connected to a blood reservoir, the height of which could be adjusted by a pulley mechanism. Changing the height of the reservoir altered the filling pressure of the left ventricle, thus providing a way of controlling mean arterial blood pressure.

A unipolar pacing lead was sutured to the left ventricular free wall, as were two additional leads for measuring a bipolar surface electrogram.

The right and left common carotid arteries were isolated. These were clamped at several times during the experiment to assess the status of the baroreflexes.

Experimental protocol. The objective of our experimental work was to obtain canine aortic input impedance spectra under a wide variety of conditions. Impedance spectra were derived from analysis of aortic pressure and flow signals digitized (50-Hz sampling rate) during 4-min periods of random ventricular pacing using spectral analysis, as described for the arterial system by Taylor (24) and reviewed below. The first random run was obtained with reflexes intact and the atrial reservoir height adjusted so that mean arterial blood pressure was between 100 and 130 mmHg. Then the baroreflexes were blocked with hexamethonium (15 mg/kg iv). Blockade was confirmed by the demonstration of no response in blood pressure to bilateral common carotid occlusion for 30 s; if a response was noted an additional 5 mg/kg was administered, and the procedure was repeated until there was no response. The reflexes were rechecked at ~1-h intervals, and additional hexamethonium was administered if necessary. Vasodilation and arterial depression occurred rapidly with the administration of hexamethonium, and therefore it was necessary to raise the atrial reservoir to keep mean blood pressure >80 mmHg. A random run was recorded in this state of vasodilation and then after vasoconstriction with either phenylephrine (40–100 μg/min) or epinephrine (5–10 μg/min). In addition, runs were taken at constant vasoconstrictor doses but with mean arterial pressure altered by changing the level of the atrial reservoir. The experiments were usually ended by ventricular fibrillation occurring during random pacing that could not be converted to normal sinus rhythm. In all, we determined 31 impedance spectra from the five dogs. Thus we obtained data over a wide range of vasoconstrictive states and mean arterial blood pressures.

Calculation of impedance. Aortic input impedance was calculated from the digitized aortic pressure and flow signals obtained during random ventricular pacing. The random data were sampled at a rate of 50 Hz for a total period of 204.80 s (3.41 min) that was subsequently divided into five nonoverlapping 40.96-s bins [2^{11} (2,048) points in each bin] of pressure and flow data so that coherence spectra could be calculated. Each bin was analyzed in the following way. In the first step, the aortic pressure (AoP) and flow (AoF) data were windowed with a Hanning window and then Fourier transformed using a Radix-2 FFT algorithm. Second, the power of the AoP ($|\mathrm{AoP}(\omega)|^2$) and the cross-power between AoP and AoF [$(\mathrm{AoF}(\omega)\cdot\mathrm{AoP}^*(\omega)$] were calculated for each bin separately and then averaged over the five bins. The impedance [$Z(\omega)$] is equal to

$$Z(\omega) = \frac{\overline{|\mathrm{AoP}(\omega)|^2}}{\mathrm{AoF}(\omega)\cdot\mathrm{AoP}^*(\omega)} \qquad (1)$$

where * denotes complex conjugate, and the lines above the power terms indicate mean values. $Z(\omega)$ is a complex number with real and imaginary parts and can be expressed in terms of a modulus and phase angle. The maximum frequency of the impedance spectrum we could calculate is determined by the sampling rate and the Nyquist criterion. Thus, with our sampling rate of 50 Hz, we could achieve a maximum frequency not >25 Hz. We chose to plot the impedance spectrum out to 20 Hz, which should minimize problems of aliasing. The resolution in the frequency domain of the impedance is determined by the reciprocal of the bin duration. In our case, with bins of 40.96 s, we could obtain an impedance point approximately every 0.025 Hz.

We also calculated the frequency-dependent coherence spectrum [$\gamma(\omega)$], which provides an index of the extent to which the AoF(ω) and AoP(ω) at each value of ω are correlated to each other during the data acquisition period. The coherence is mathematically defined as

$$\gamma(\omega) \equiv \left\{ \frac{\overline{|\mathrm{AoF}(\omega)\ \mathrm{AoP}^*(\omega)|^2}}{\overline{|\mathrm{AoP}(\omega)|^2}\ \overline{|\mathrm{AoF}(\omega)|^2}} \right\}^{1/2} \quad (2)$$

$\gamma(\omega)$ varies between 0 and 1. In the presence of biological variation, system nonlinearity, or other sources of random noise, the coherence function becomes less than unity; the closer to unity, the more correlated are the AoP and AoF, and consequently, the more reliable the estimate of the impedance value at that frequency. Therefore we excluded impedance values that had a coherence <0.8 (an arbitrary cutoff point). By use of this arbitrary cutoff, we excluded ~10% (on average) of the data points, and these points were predominantly at frequencies >10 Hz.

After calculation of the impedance spectrum, we corrected the phase angle [$\phi(\omega)$] to account for the fact that the flowmeter signal has a fixed 8-ms time delay

$$\phi_c(\omega) = \phi(\omega) - \omega \cdot 008 \text{ (s)} \quad (3)$$

where $\phi_c(\omega)$ is the corrected phase angle, and angles are expressed in radians.

Determination of best-fit Windkessel parameters. The three parameters of the Windkessel model, depicted in Fig. 1, that best fit each measured spectrum were obtained as follows. R_c was set equal to the arithmetic mean magnitude of all the impedance data collected above 2 Hz. This definition has been proposed previously by others (10, 11, 15). The peripheral R_a was taken as the difference between the measured direct current (DC) resistance (i.e., the modulus of the impedance at 0 Hz) and R_c. To estimate C_a, we used a method outlined recently by Yin (28) specifically for the Windkessel model. This method assumes that the system is linear (i.e., the compliance is independent of arterial pressure) but does not require the assumption that the decay of the arterial pressure is strictly exponential, that is, it allows for the presence of wave reflections. The time constant of decay of the arterial pressure during diastole is estimated by

$$\tau = A_{12}/(P_1 - P_2) \quad (4)$$

where A_{12} is the integral over the time period from t_1 to t_2 of the arterial pressure wave, P_1 is the arterial pressure at t_1, and P_2 is the arterial pressure at t_2; t_1 is chosen to occur slightly after ejection has ended and t_2 before the next ejection starts. Once τ is determined, C_a is obtained by

$$C_a = \tau/R_a \quad (5)$$

For each set of random data we made five determinations of τ by this method at different times throughout the 4-min period of acquired data. These separate determinations were always very close to each other (<±10% variation from the mean), and the mean value was used for all pertinent calculations.

Loading a model ventricle with a real impedance spectrum (computer simulation). Our purpose in executing this computer simulation was to compare the coupling of a model left ventricle to a real aortic impedance with the coupling of the same ventricular model to the Windkessel model with parameter values adjusted to best approximate that real impedance. Because the properties of the model left ventricle are clearly specified and constant, a straightforward comparison between the two arterial loads can be made. The details of exactly how a computer-simulated ventricle was coupled to real impedance spectra is provided in APPENDIX 1. Very briefly, the ventricular model was an extension of the previously proposed time-varying elastance model of ventricular contraction (20). End-systolic ventricular properties were characterized by the slope (E_{max}), and the volume-axis intercept (V_0), of the linear end-systolic pressure-volume relationship. At end diastole, the ventricular pressure-volume relationship was considered to be exponential, with a constant of proportionality A and exponential constant B. During contraction, ventricular properties made a smooth transition between end-diastolic and end-systolic pressure-volume relations according to a time function, designated $\alpha(t)$. End-systolic properties were attained at time T_{max} during the cardiac cycle. We also investigated how an internal ventricular resistance (R_i) (5, 17) would effect the comparison between real and Windkessel impedances.

Figure 2*A* shows the circuit for loading the simulated ventricle, symbolized by the variable capacitor $E(t)$ to the measured afterload impedance, $Z(\omega)$ (AoV represents the aortic valve). To perform the mathematical calculations required to accomplish this coupling, it was necessary to decompose the original impedance $Z(\omega)$ into a series resistance, R_c, and a peripheral impedance, $Z'(\omega)$, as shown in Fig. 2*B* (the circuits of *A* and *B* are mathematically equivalent). To make calculations in the time domain, we determined the Fourier transform of the impedance spectrum $Z'(\omega)$, which is the impulse response [designated $z'(t)$] of the peripheral arterial system. Finally, simulated arterial pressure was determined by calculating the convolution integral between the flow across R_c and $z'(t)$. The details of how the impulse response and convolution integral were calculated are detailed in APPENDIX 1.

As shown in Fig. 2, the ventricle was filled during diastole by a pressure source (P_v) through a resistance (R_v) and the mitral valve (MV).

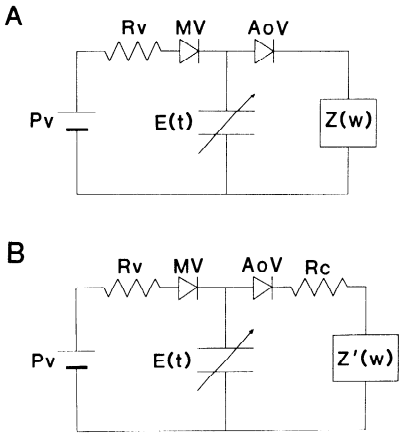

FIG. 2. *A*: we executed a computer simulation to impose an arbitrary afterload impedance $Z(\omega)$ on a model left ventricle with properties $E(t)$. Other elements in simulation are aortic valve (AoV), mitral valve (MV), preload filling pressure (P_v), and resistance to venous filling, R_v. *B*: for computational purposes it was advantageous to decompose impedance $Z(\omega)$ into a series resistance (R_c) and a modified impedance $Z'(\omega)$, which is determined as described in *Eq. A10* and described in text. Afterload impedances in *A* and *B* are identical.

Validation of computer simulation. In view of the extensive mathematical handling of the original data, we wanted to validate that the computer simulation of A-V coupling by use of the impulse-response method indeed imposed the desired impedance spectra on the model ventricle. To accomplish this test we loaded the model ventricle with an experimentally determined impulse response, and we mimicked random pacing in the simulation and redetermined from the simulated data the aortic input impedance in the same manner as described above for acquisition of the real data. This procedure is detailed in APPENDIX 2. The results (see Fig. 9) indicated that the simulation did impose the desired impedance on the model ventricle with sufficient accuracy for the comparisons to be made in the present study.

Comparison between A-V coupling with real and best-fit Windkessel afterload. The model ventricle was coupled to each of the measured impedance spectra and their corresponding Windkessel models. For each pair, we compared the following coupling variables: stroke volume, stroke work, peak aortic flow, arterial systolic, diastolic and mean blood pressures, and finally the pressure-volume area. The pressure-volume area is the area on the pressure-volume diagram bounded by the end-systolic pressure-volume relation, the end-diastolic pressure-volume relation, and the systolic portion of the pressure-volume loop drawn by a contraction from a given volume. The pressure-volume area has been shown to correlate with myocardial oxygen consumption when the myocardium is in a constant contractile state (19). This comparison was carried out for all spectra, with the parameters describing ventricular function set at what would be considered to be within the normal range for a 20-kg dog: an E_{max} of 6 mmHg/ml, heart rate of 100 beats/min, T_{max} of 175 ms, V_0 of 5 ml, A of 0.65 mmHg, B of 0.09/ml (A and B being the parameters describing diastolic properties, as detailed in *Eq. A7* of the APPENDIX 1), and a filling pressure of 7.5 mmHg (these values of A, B, and P_v provided a preload volume of 33.1 ml). In addition, we arbitrarily chose 10 of the spectra and made the comparison at different heart rates (70, 130, and 160 beats/min), and we chose an additional 10 of the spectra and made the comparison at different E_{max} values (4 and 9 mmHg/ml). Our analysis showed that neither changes in heart rate nor E_{max} influenced our quantitative conclusions and will not be discussed further.

RESULTS

Real vs. Windkessel impedance spectrum and impulse response. A canine aortic input impedance spectrum that was typical of those we obtained by white noise analysis is illustrated in Fig. 3 (·····). This spectrum was obtained from a 22-kg dog before blockade of baroreflexes. Except for a few points, the coherence (*top*) is always very close to unity, indicating a high degree of mathe-

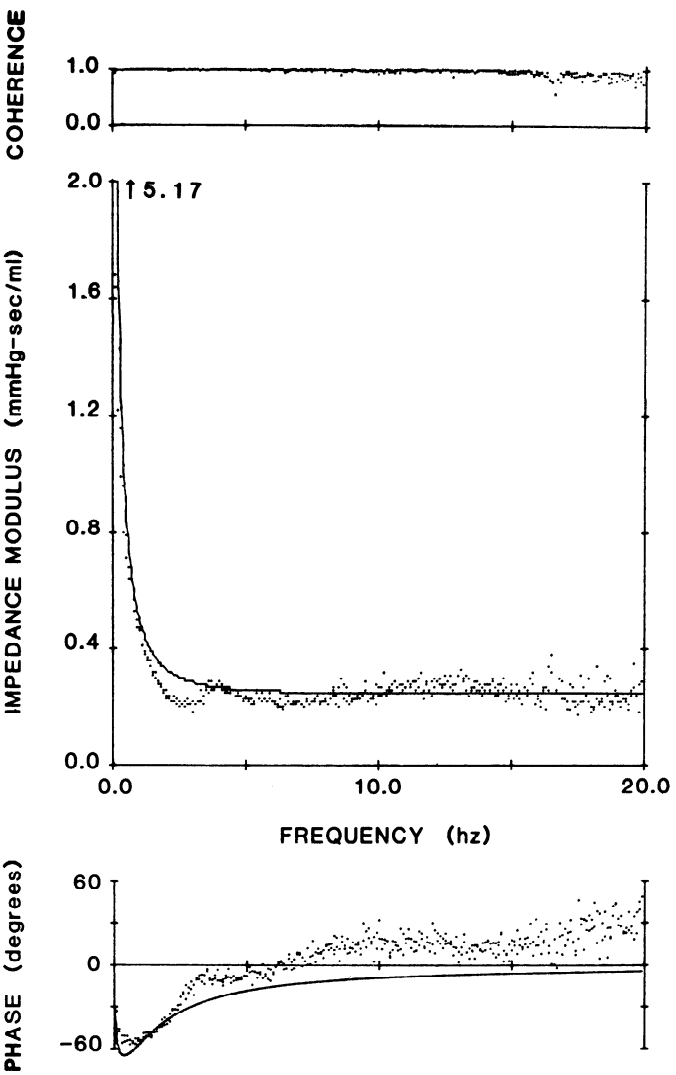

FIG. 3. Typical experimentally determined impedance spectrum (·····) with corresponding best-fit Windkessel (——). Coherence (*top*) is very close to 1 up to ~17 Hz at which point there is some deviation. Moduli of impedances are shown in *middle*, and phases are presented in *bottom*. Note that scaling of y-axis was set to provide adequate resolution of spectrum at higher frequencies and that very low-frequency points are not within this range; therefore, moduli of the spectra at 0 Hz, 5.17 mmHg·s·ml^{-1}, is off the scale of graph. Detailed explanations provided in text.

matical certainty in the measured impedance values out to 20 Hz. The impedance of the best-fit Windkessel model is also depicted (——) (R_a = 4.92 mmHg·s·ml^{-1}, R_c = 0.25 mmHg·s·ml^{-1}, C_a = 0.37 ml/mmHg). The modulus (*middle*) of the real impedance starts at a DC resistance of 5.17 mmHg·s·ml^{-1}, declines to a minimum at ~2.9 Hz, and exhibits low-amplitude oscillations around R_c. Although the modulus of the corresponding Windkessel impedance starts at the same DC resistance and settles at the same value at higher frequencies, it exhibits neither a minimum at 2.9 Hz nor any oscillations. The phase (*bottom*) of the real impedance starts at 0°, declines to a minimum of −55° at 0.74 Hz, ascends in a biphasic manner to a 0° crossing at ~6.2 Hz, and continues to rise in a monotonic manner to a plateau of ~20°. The phase of the corresponding Windkessel impedance starts at 0°, reaches a minimum of −63° at 0.63 Hz, and then increases monotonically toward 0°.

In all, we obtained 31 impedance spectra from the 5 dogs studied. For the group as a whole, values of R_a ranged between 2.25 and 9.21 (mean 4.83) mmHg·s·ml^{-1}, R_c ranged between 0.14 and 0.36 (mean 0.25) mmHg·s·ml^{-1}, and C_a ranged between 0.20 and 0.90 (mean 0.39) ml/mmHg. The frequency at which the phase crossed through 0° varied between 5.0 and >20.0 (mean 9.8) Hz, and the phase of the impedance at 20 Hz ranged between −20 and +57° (mean +10°). The frequency of the first minimum in the impedance modulus ranged between 1.6 and 6.6 (mean 2.9) Hz. A detailed analysis of the influence of the various physiological interventions on the characteristics of the impedance spectra is not within the scope of the present analysis.

As described in APPENDIX 1, it was required that the impedance spectrum be padded out to 100 Hz to determine the impulse response. In Fig. 4 (*top*) it is demonstrated how the measured spectrum plotted in Fig. 3 was padded. As described in APPENDIX 1, the modulus was assumed to be equal to the characteristic impedance, and the phase was assumed to monotonically approach 0°. In Fig. 4 (*bottom*), we show the calculated impulse response (after having subtracted off the value of R_c from the original impedance spectrum as described in *Eq. A10*) for the real data (——) and for the best-fit Windkessel (----). Note that the units of the impulse response are millimeters of mercury per milliliter. The real impulse response exhibits marked oscillations near the beginning, a rapid decay, and low-amplitude oscillations about a small positive value of ~0.14 mmHg/ml. In Fig. 4 (*inset*) the same signals (shown with expanded scales) more clearly demonstrate the large-amplitude negative-going spike at the onset of the impulse response. In contrast, the impulse response of the Windkessel model rises rapidly to its highest value and declines monoexponentially over its entire course with a time constant equal to $R_a \cdot C_a$, which in this case equals 1.83 s.

A-V coupling. The physiological signals presented in Fig. 5 were obtained when the simulated ventricle (with "control" parameter values) was loaded with the impulse responses of the real and best-fit Windkessel impedances of Fig. 3. The AoP, left ventricular pressure, left ventricular volume, and AoF are shown in Fig. 5 (*left*); the solid

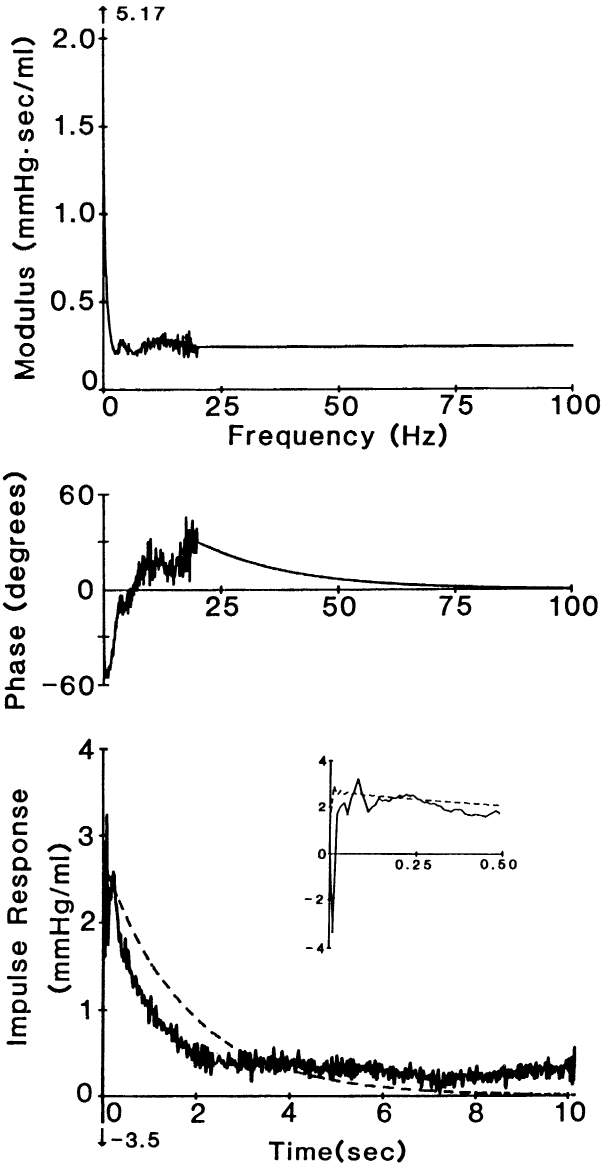

FIG. 4. Demonstration of how impedance modulus (*top*) and phase (*middle*) of spectrum presented in Fig. 3 were extended to a maximum frequency of 100 Hz. Modulus was assumed to be equal to characteristic impedance, and the phase was assumed to monotonically approach 0°. Impulse response of extended real impedance spectrum (——) and that of corresponding Windkessel, after having subtracted off characteristic impedance (*Eq. A10*), are shown at the *bottom*. *Inset*: first 0.5 s of the same impulse responses are shown with an expanded negative scale, clearly revealing single negative point of real impulse response.

lines depict signals obtained with the real impedance, and the dashed lines depict signals obtained with the Windkessel afterload. The corresponding pressure-volume loops are shown in Fig. 5 (*right*). Note the end-systolic and end-diastolic pressure-volume relations depicted in the figure. AoP obtained with the Windkessel afterload decayed with a simple exponential time course after ejection ends. With the real impedance, AoP increased initially after end ejection, and the decay during diastole was not exponential; relatively large wave reflections are noted, and AoP was generally higher throughout diastole. The differences in the left ventricular pressure tracings result from the differences in the time course of ejection. As noted in the left ventricular volume tracing

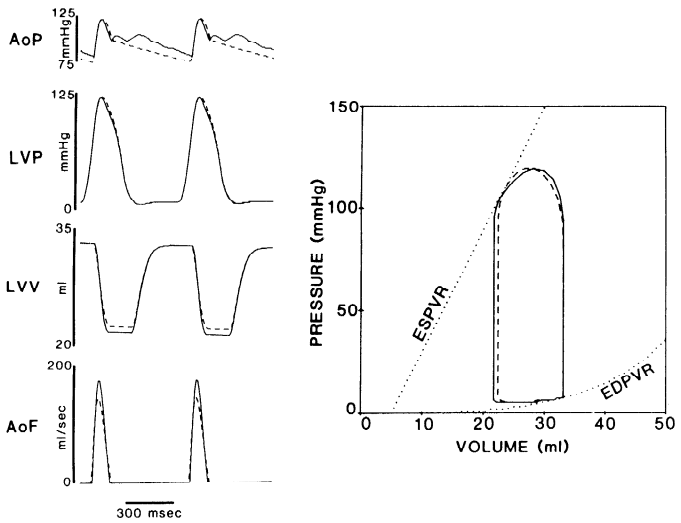

FIG. 5. Physiological signals obtained from computer simulation by coupling of model ventricle to impedance spectrum shown in Figs. 3 and 4 (——) and to best-fit Windkessel model (----). *Left*: the aortic pressure (AoP), left ventricular pressure (LVP), left ventricular volume (LVV), and aortic flow (AoF). *Right*: corresponding pressure-volume loops and end-systolic and end-diastolic pressure-volume relationships (ESPVR and EDPVR, respectively). AoP and AoF waveforms are quite different. Despite this, stroke volumes are only 0.7 ml different. Stroke work and pressure-volume area are also very similar with the 2 afterloads.

and its derivative the AoF, ventricular ejection flow reached a higher peak value but was of slightly shorter duration with the real load compared with the Windkessel load. Despite the noted differences there are significant similarities in the tracings: maximum and minimum AoPs were very similar as was the stroke volume, which was 0.7 ml greater with the real impedance afterload. Further similarities are identified on the pressure-volume diagram where it is noted that the stroke work (the area within the pressure-volume loop) and the pressure-volume area of the two loops are very similar.

The differences noted above for the chosen representative spectrum were similar to those observed with the other spectra both qualitatively and quantitatively. The scattergrams presented in Fig. 6 summarize the comparison between coupling the heart (with control parameter values) to the 31 experimentally determined impedances and their corresponding best-fit Windkessel afterloads; the seven coupling variables are examined. The abscissa of each point represents the value of the variable obtained with the experimentally measured impedance as afterload, and the ordinate represents the value obtained with the corresponding Windkessel impedance as afterload. Note that the dotted line in each panel is the line of identity and not the line of regression. The difference between stroke volume (SV) obtained with the real and Windkessel impedances ranged between −0.6 and +1.1 ml. On average, the SV obtained with the Windkessel model was 97% of that obtained with the real impedance afterload. Results of paired t test indicated that with this group of afterloads, the difference in SV was not statistically significant ($P > 0.2$). On average, the stroke work obtained with the real impedance was only 1% greater ($P > 0.2$), and pressure-volume area was only 1% less ($P < 0.01$) than with the Windkessel impedance (Fig. 6B). The comparison among blood pressures (Fig. 6C) indicated no statistically significant difference in systolic or diastolic pressures. Mean blood pressure was slightly (2.5 mmHg) but statistically ($P < 0.01$) greater with the real impedance. Peak AoF (Fig. 6D) was consistently and significantly ($P < 0.001$) greater with the real impedance as afterload. On average, peak flow obtained with the Windkessel afterload was only 85% of that obtained with the real impedance. These comparisons are further summarized in Table 1.

Are differences in modulus or phase responsible for differences in coupling between real and Windkessel impedances? We wanted to determine whether the differences between coupling variables obtained with real and Windkessel impedances were the result of differences in modulus spectra, phase spectra, or a combination of both. Our strategy to address this question was to alternately replace the real modulus and phase with their Windkessel counterparts, as outlined in Fig. 7. In Fig. 7 (*top*), we present the modulus of a real impedance spectrum (*left*) and of its best fit Windkessel model (*right*). In the first column we present the phase of the real impedance spectrum (*top*) and of the best-fit Windkessel model (*bottom*). In each of the four boxes of the matrix we present the impulse response of the spectrum composed of the intersecting phase and modulus. Thus the impulse response of the real impedance spectrum is presented in *box A*, that of the Windkessel spectrum is presented in *box D*, that of the spectrum composed of the Windkessel modulus and the real phase data is presented in *box B*, and the impulse response of the spectrum composed of the real modulus and the Windkessel phase data is presented in *box C*. By comparing the coupling variables that resulted from afterloads A and C, we can assess the role of the differences in phase between real and Windkessel afterloads, since the moduli are the same for these two cases. Similarly, by comparing the coupling variables that resulted from afterloads A and B we can assess the role of the differences in moduli. The values of the coupling variables obtained with each of these impulse responses are summarized in Fig. 8. For example, the SV obtained with the real impedance (*box A*) was 11.2 ml, whereas that obtained with the best-fit Windkessel (*box D*) was 10.3 ml, a difference of 0.9 ml. When the real modulus and the Windkessel phase were combined (*box C*), the resulting SV was 10.7 ml, a difference of only 0.5 ml from SV with the real impedance. When the Windkessel modulus and the real phase were combined (*box B*), the resulting SV was 10.6 ml, a difference of only 0.6 ml from that with the real impedance. Thus substitution of the real phase by the Windkessel phase did not entirely resolve the difference in coupling between real and Windkessel afterloads nor did substitution of the real modulus by the Windkessel modulus.

A majority of the difference in maximal AoF observed between the real and the Windkessel afterload was accounted for by substitution of the Windkessel phase for the real phase (Fig. 8C). The difference in stroke work was resolved by substitution of the Windkessel modulus for the real modulus (Fig. 8B). The differences in the remaining coupling variables (pressure-volume area, sys-

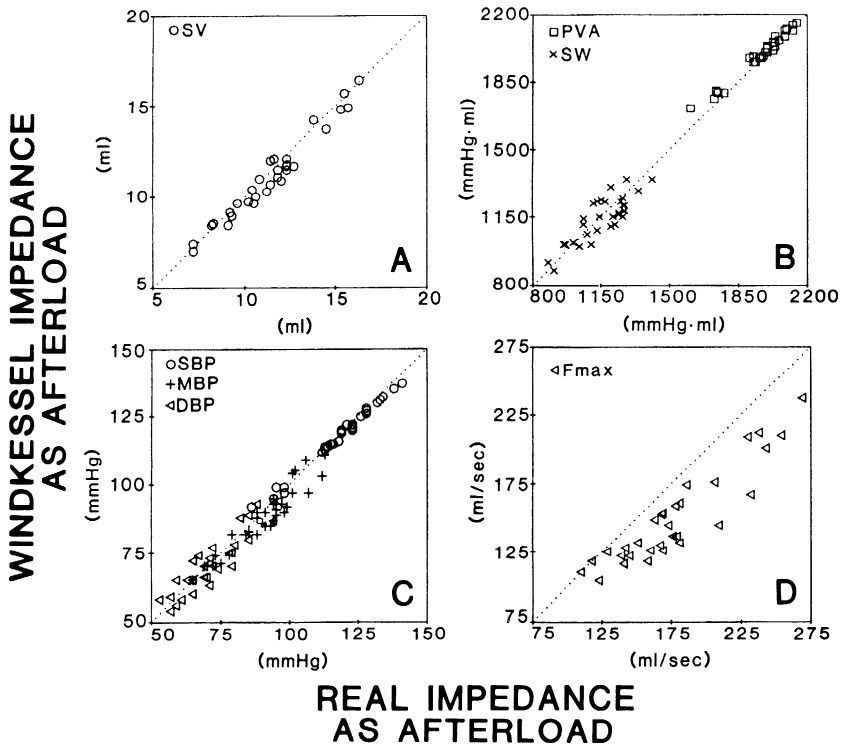

FIG. 6. Summary of difference between real and best-fit Windkessel afterloads as examined by 7 coupling variables: stroke volume (SV), pressure-volume area (PVA), stroke work (SW), systolic, mean, and diastolic aortic pressure (SBP, MBP, and DBP, respectively), and peak aortic flow (F_{max}). Ordinant of each point is value of coupling variable obtained with real impedance as afterload, and abscissa represents its value with best-fit Windkessel as afterload. ·····, Line of identity. A statistical analysis of the differences is presented in Table 1.

TABLE 1. *Comparison of mean values of coupling variables obtained with real and Windkessel afterloads*

Variable	Mean Value With		*P*
	Real impedance afterload	Windkessel impedance afterload	
SV	11.4 ml	11.1 ml	>0.2
F_{max}	177 ml/s	149 ml/s	<0.001
SW	1,148 mmHg·ml	1,137 mmHg·ml	>0.2
PVA	1,958 mmHg·ml	1,978 mmHg·ml	<0.01
SBP	118.3 mmHg	117.7 mmHg	>0.1
MBP	90.7 mmHg	88.2 mmHg	<0.01
DBP	71.1 mmHg	70.7 mmHg	>0.1

SV, stroke volume; F_{max}, maximum flow; SW, stroke work; PVA, pressure-volume area; SBP, systolic blood pressure; MBP, mean blood pressure; DBP, diastolic pressure. * Statistical analysis by paired *t* test.

tolic blood pressure, diastolic blood pressure, and mean blood pressure) were dependent on differences in both phase and modulus between real and Windkessel spectra.

From this analysis we can conclude that differences in both phase and modulus spectra between real and Windkessel impedances contribute to the differences in A-V coupling with the two afterloads. This analysis was carried out for an additional four spectra, and the results supported the same conclusion.

Influence of ventricular R_i. For 10 of the measured impedance spectra we assessed the differences between real and Windkessel afterloads when the model of the ventricle was extended beyond the simple time-varying elastance to also include an R_i (see *Eq. A9b* in APPENDIX 1). Results that summarize the influence on SV are presented in Table 2. Table 2 shows the influence of R_i on the difference between SV obtained with the best-fit Windkessel as afterload (SV_W) and with the real impedance as afterload (SV_R). For the spectra tested, SV decreased an average of 4.3% when R_i was present. However, as shown in Table 2, $SV_W - SV_R$ was almost the same with and without R_i. There was a similar lack of influence of ventricular R_i on our assessment of the Windkessel on all the other variables examined.

DISCUSSION

Significant advances have been achieved during the past 20 years in characterizing, quantitatively, ventricular and arterial properties. However, theoretical advances in our understanding of the coupling between the ventricle and the arterial system (A-V coupling) are largely dependent on the validity of relatively simple models of aortic input properties, such as the three-element Windkessel model, which have been developed to facilitate both the theoretical analysis and experimental exploration of cardiovascular function (1, 3, 4, 22, 23, 25, 26). It was the aim of the present study to assess the validity of the Windkessel model (Fig. 1) as a descriptor of aortic input impedance for the purpose of studying A-V coupling. Previous efforts along this line have been limited predominantly to qualitative comparison of the real and Windkessel impedance spectra. Our approach was to compare the coupling of a computer-simulated ventricle to experimentally determined impedance spectra and to the Windkessel models that most closely reproduced those real impedances.

The differences between the real and Windkessel impedance spectra are well-known, as are the differences between the real and the Windkessel impulse responses; typical comparisons are presented in Figs. 3 and 4. It has also been noted, although qualitatively, that the AoP and AoF waveforms obtained with the real and Windkessel spectra are different (as evident in Fig. 5). The new information provided by the present study focuses on a

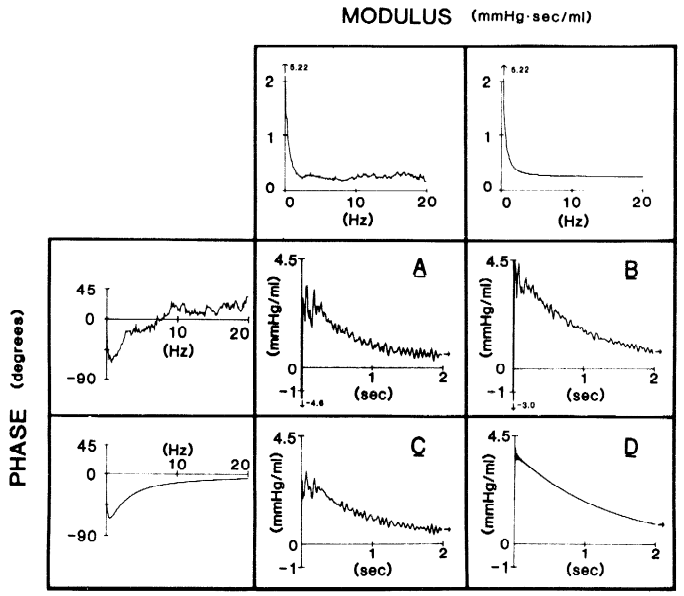

FIG. 7. *Top*: impedance moduli of real and best-fit Windkessel. *First column*: impedance phases of real and best-fit Windkessel. In each box (*A–D*), impulse response of impedance spectrum composed of modulus in same column and phase in same row. For example, in *box C* is impulse response of impedance composed of real modulus and Windkessel phase. The purpose of combining phase and modulus data in this fashion was to determine whether differences in coupling variables between real and best-fit Windkessel were a result of differences in phases, moduli, or a combination of both. See Fig. 8 for comparison of coupling variables.

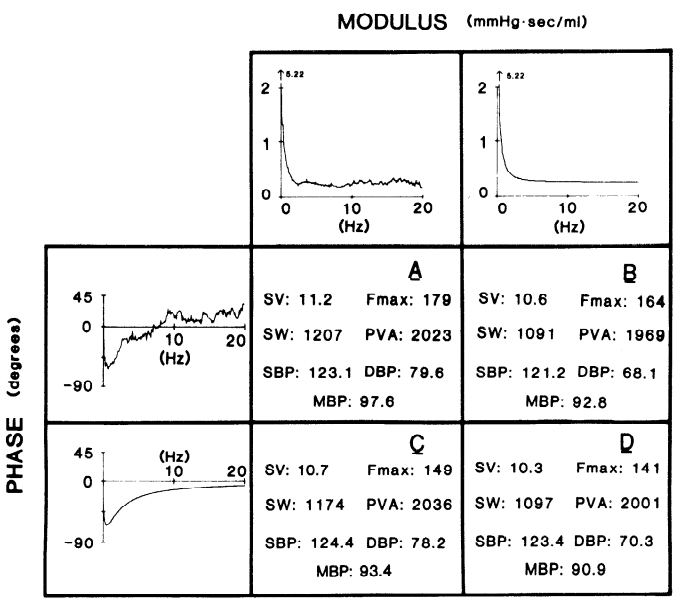

FIG. 8. Summary of coupling model ventricle to different impulse responses presented in Fig. 7. *A*: coupling variables obtained with real impedance; and *D*: coupling variables obtained with Windkessel impedance. As shown, substitution of Windkessel modulus for real modulus (comparing *A* and *B*) or substitution of the Windkessel phase for the real phase (comparing *A* and *C*) has an effect on coupling variables. This indicates that differences in both the phases and moduli between real and Windkessel impedance have an impact on aortic-ventricular coupling. SV, stroke volume; SW, stroke work; SBP, systolic blood pressure; F_{max}, maximum flow; PVA, pressure-volume area; DBP, diastolic blood pressure; MBP, mean blood pressure.

TABLE 2. *Influence of internal ventricular resistance on assessment of Windkessel model as a descriptor of afterload impedance*

Experiment	$SV_W - SV_R$	
	Without internal resistance	With internal resistance
1	−0.53	−0.43
2	−0.39	−0.40
3	−0.78	−0.96
4	−0.25	−0.34
5	−0.37	−0.48
6	0.00	0.04
7	0.16	0.32
8	−0.53	−0.67
9	0.04	0.33
10	−0.21	−0.26

SV_W, stroke volume obtained with best-fit Windkessel; SV_R, stroke volume obtained with real impedance. All values in units of milliliters.

quantitative comparison between coupling variables obtained with real and Windkessel impedances.

Peak AoF obtained with the Windkessel afterload was (on average) 85% of that obtained with the real impedance. Differences in other coupling variables, such as SV, stroke work, systolic blood pressure, or diastolic blood pressure between real and Windkessel afterloads, were small in magnitude and not statistically significant. A small (~1%) but statistically significant difference in pressure-volume area (and therefore, theoretically, on oxygen consumption) and mean AoP were noted. In specific cases, however, differences in the coupling variables were as large as 10% (see Fig. 6).

By the combination of real and Windkessel moduli and phase data (Figs. 7 and 8), we could demonstrate that in general the differences noted in coupling variables resulted from differences that existed in both the phases and moduli between the real and Windkessel spectra.

These conclusions were not altered when ventricular contractility or heart rate were changed in the simulation. Nor were the results influenced by the presence of a ventricular R_i (5, 17).

The use of the impulse response for purposes of characterizing arterial properties and simulating A-V coupling has been explored previously (7, 8, 16, 18). In those studies, the impulse response was obtained by inverse Fourier transform of discrete impedance spectra, i.e., from spectra in which impedance values were only available at frequencies that were harmonics of the heart rate. Thus A-V coupling could only be studied at the heart rate at which the original impedance spectrum was determined. This was not the case in the present study, since we obtained impedance spectra with high resolution in the frequency domain. Common to previous efforts, however, we were faced with the problem that the impedance spectrum could only be determined up to a maximum frequency of ~20 Hz. However, inverse Fourier transformation of an impedance spectrum with a maximum frequency of 20 Hz would not permit adequate resolution of the impulse response in the time domain to simulate A-V coupling. We overcame this problem by padding the impedance spectra to 100 Hz in a physiologically reasonable way. From a theoretical viewpoint, even

if the assumptions we made in padding the spectra were not fully justifiable, the fact that the vast majority of the power of AoF falls within the first 10 harmonics of the heart rate suggests that the exact nature of the impedance spectrum at frequencies >20 Hz (even at a heart rate of 160 beats/min) should have little impact on A-V coupling.

In our study we evaluated the accuracy of only the simple three-element Windkessel model for describing afterload impedance. Other more complicated models of aortic input properties have been proposed (see Refs. 6, 12, and 27 for examples). Many of these models are further modifications of the Windkessel and include such elements as inductors, nonlinear (pressure dependent) resistance, and compliance elements in various arrangements. The impedance spectra of most of these models, especially those containing a series inductance, are known to deviate from real aortic impedance at frequencies above ~10 Hz (where the impedance magnitude increases continuously) and could not be evaluated as in the present study. Other types of models based on reflected waves in tubes have been investigated and they seem to provide great flexibility in reproducing realistic impedance spectra (14). Although an investigation of other more complex models of afterload impedance is clearly warranted, one should also keep in mind that it is the simplicity of the three-element Windkessel model that has facilitated an advancement in our understanding of A-V coupling (1, 4, 7, 22, 23).

In the present study we have compared A-V coupling with Windkessel impedance spectra with A-V coupling with experimentally determined impedance spectra obtained from presumably healthy dogs of random ages. Studies in both canine and human subjects have shown how aortic input impedance is modified by the normal age process (11), by chronic states of congestive heart failure (15), and by hypertension (26). In those studies, emphasis is placed on alterations in the magnitude and frequency of oscillations in the impedance modulus and the frequency at which the phase crosses back through 0°; these features of the impedance spectrum are related to the occurrence and timing of vascular wave reflections. The benefits of reflections occurring at the proper time (which may serve to unload the heart during ejection) have been discussed for the normal conditions, as have the potential adverse effects of either enhanced or diminished reflections in pathophysiological states. We found that the influence of such wave reflections on all coupling variables except the maximum AoF was relatively little (<10%). Accordingly, it is possible that alterations in the fine details of the impedance spectra may not have a significant effect on A-V coupling (i.e., SV, stroke work, myocardial oxygen demand, and arterial blood pressure), rather, alterations in A-V coupling appear to be dominated by the gross features of the impedance spectrum such as the R_a, C_a, and R_c. This is not to say, however, that such alterations are of no significance, since it is possible that they might have some important secondary effects, such as an influence on ventricular performance via altered ejection pattern or diastolic aortic pressure or on the long-term adaptive response of the myocardium. Furthermore, even though we did obtain impedance spectra from a very wide range of mean blood pressures (approximate mean pressures between 70 and 170 mmHg) and states of vascular tone (produced by hexamethonium vasodilation and phenylephrine vasoconstriction), the extent to which the features of the impedance spectrum were altered by our acute interventions may not fully cover those encountered under chronic diseased states. Thus we caution against extrapolation of the results of our comparison between real and Windkessel afterloads to A-V coupling in pathophysiological conditions.

In regard to our analysis, we should point out the possibility that our results may be somewhat dependent on the model used to simulate ventricular function. Specifically, if the contractile properties of a real ventricle are very different than those of the simulated ventricle then the nature and extent of the deviations in coupling between real and Windkessel impedances may be different in situ than we have assessed. Even though this possibility must be acknowledged, the fact that our analysis was little affected by the presence or absence of an internal ventricular resistance (which markedly alters the ejection pattern) speaks to a relative insensitivity of our analysis to the ventricular model. Still, there may be many ways in which real ventricular properties differ from those imparted to our simple model that may affect the comparison.

Conclusions. Results of previous studies have clearly demonstrated the utility of the three-element Windkessel as a model of aortic input impedance for simplifying the analysis of A-V coupling. Our analysis indicates that with a simulated ventricle, most of the coupling variables examined were not significantly different between real and best-fit Windkessel afterloads. The major differences existed in the contours of the AoF and pressure waves (this has been recognized previously), and there were also significant differences in peak AoF. Thus the decision of whether the Windkessel model adequately describes aortic input impedance depends on the purpose for which it is to be used. If SV, stroke work, or oxygen consumption are the variables of interest, then the Windkessel may be sufficient, whereas for prediction of peak AoF, AoF, or pressure contours it is clearly insufficient.

APPENDIX 1

In this section we provide the details of *1*) the model used to simulate ventricular function, *2*) the method of coupling the simulated heart and measured arterial impedance, and *3*) how the peripheral arterial system impulse response was calculated from the measured impedance spectra.

Ventricular model. The model we used to represent ventricular function is an extension of the previously proposed time-varying volume-elastance model [$E(t)$] that describes the relation between instantaneous ventricular volume [V] and left ventricular pressure [P_{LV}] (20). The present model assumes a linear end-systolic pressure-volume relationship, a nonlinear end-diastolic pressure-volume relationship, and a smooth progression between the two during the cardiac cycle. Thus end-systolic pressure (P_{es}) and V are interrelated by

$$P_{es}(V) = E_{max}[V - V_0] \qquad (A6)$$

where E_{max} is the maximal volume elastance, and V_0 is the

volume at which end-systolic pressure is 0 mmHg. End-diastolic pressure (P_{ed}) and volume are interrelated by

$$P_{ed}(V) = A[e^{B(V-V_0)} - 1] \quad (A7)$$

where A and B are constants, and V_0 has the same value as in *Eq. A6*. Finally, we define a time function $\alpha(t)$ that describes the time course with which the chamber stiffness varies between end systole (*Eq. A6*) and end diastole (*Eq. A7*)

$$\begin{aligned} \alpha(t) &= 0.5\left[1 + \sin\left(\frac{180t}{T_{max}} - 90°\right)\right] \qquad 0 < t < 2T_{max} \\ &= 0 \qquad\qquad 2T_{max} \le t \le T \end{aligned} \quad (A8)$$

where t is the time from the onset of systole, T_{max} is the time to the end of systole, and T is the duration of the cardiac cycle. Thus $\alpha(t)$ has a volume of 0 at end diastole (when $t = 0$ or when $t = T$) and a value of unity at end systole (when $t = T_{max}$). *Equations A6, A7,* and *A8* can be combined to describe the instantaneous relationship between ventricular volume and pressure

$$P_{LV}[V(t), t] = \alpha(t)\{P_{es}[V(t)] - P_{ed}[V(t)]\} + P_{ed}[V(t)] \quad (A9a)$$

Accordingly, ventricular function is characterized by the parameters E_{max}, T_{max}, V_0, A and B, and the function $\alpha(t)$. Note that with this formulation, the ventricular end-systolic pressure-volume relationship is totally independent of afterloading conditions. We also investigated the effect that internal ventricular resistance (5, 17) would have on our comparison between real and Windkessel spectra. In those cases, P_{LV} was determined from *Eq. A9b*

$$P_{LV}[V(t), t] = \alpha(t)\{P_{es}[V(t)] - P_{ed}[V(t)]\} + P_{ed}[V(t)] - R_iF(t) \quad (A9b)$$

where R_i is the internal ventricular resistance and is a function of instantaneous P_{LV} (5, 17), and $F(t)$ is the instantaneous flow out of the ventricle. The value of the pressure-dependent R_i is determined as described previously by the ratio between the instantaneous $P_{LV}(t)$ and a fixed value called F_{max} (maximum flow), which in our calculations was set equal to 700 ml/s: $R_i = P_{LV}(t)/F_{max}$ (see Refs. 5 and 17 for further details about ventricular R_i).

Coupling ventricle and arterial system. Coupling the simulated ventricle, represented in Fig. 2*A* by the capacitor with time-varying properties symbolized by $E(t)$, to the desired impedance, $Z(\omega)$, in the presence of the aortic valve (AoV) was accomplished by numerical methods similar to those described by Latson et al. (7), and schematized in Fig. 2*B*. Briefly, the desired impedance $Z(\omega)$ (a complex number) was decomposed into a series resistance analogous to R_c in the Windkessel model and a modified impedance denoted $Z'(\omega)$. The reason for performing this decomposition will be discussed. $Z'(\omega)$ was calculated by subtracting the value of R_c from the real part of the original $Z(\omega)$, that is

$$\begin{aligned} \mathrm{Re}[Z'(\omega)] &= \mathrm{Re}[Z(\omega)] - R_c \\ \mathrm{Im}[Z'(\omega)] &= \mathrm{Im}[Z(\omega)] \end{aligned} \quad (A10)$$

where Re[ ] denotes the real part and Im[ ] denotes the imaginary part. Thus the impedance of the afterload circuits in Fig. 2, *A* and *B* are mathematically identical. The topology of the circuit in Fig. 2*B* has the advantage over the circuit in Fig. 2*A* in that it allows for calculation of the flow into the aortic root (AoF) at any instant in time as

$$\begin{aligned} \mathrm{AoF}(t) &= (P_{LV}(t) - \mathrm{Pa}(t))/R_c \qquad P_{LV} > \mathrm{Pa} \\ &= 0 \qquad\qquad P_{LV} \le \mathrm{Pa} \end{aligned} \quad (A11)$$

where $\mathrm{Pa}(t)$ is the pressure across the impedance $Z'(\omega)$. $\mathrm{Pa}(t)$ is calculated in the time domain by convolution of the aortic flow signal with the inverse Fourier transform of $Z'(\omega)$ (called the impulse response of the arterial system), denoted $z'(t)$

$$\mathrm{Pa}(t) = \int_0^t z'(t - \sigma)\ \mathrm{AoF}(\sigma)\mathrm{d}\sigma \quad (A12)$$

where σ is an integration variable. This integral was evaluated digitally by Euler's method. Furthermore, as described below, the duration of the impulse response was truncated at 10.24 s so that in practice the integral was evaluated over the time interval between t and 0 s for $t < 10.24$ s and between t and $t - 10.24$ s for $t > 10.24$ s.

Aortic pressure, $\mathrm{AoP}(t)$, is determined by

$$\mathrm{AoP}(t) = \mathrm{AoF}(t) \cdot R_c + \mathrm{Pa}(t) \quad (A13)$$

Instantaneous ventricular volume is determined by integration of AoF and flow into the ventricle during diastole supplied by the simple pressure source-resistance-mitral valve circuit shown in Fig. 2 (P_v, R_v, and MV, respectively). Once ventricular volume is determined, ventricular pressure can be calculated from *Eq. A9a* or *Eq. A9b*. All calculations for the simulation were carried out on an IBM PC equipped with an 8087 math coprocessor chip.

Generation of impulse response. The impulse response [$z'(t)$] was determined by taking the inverse Fourier transform of the

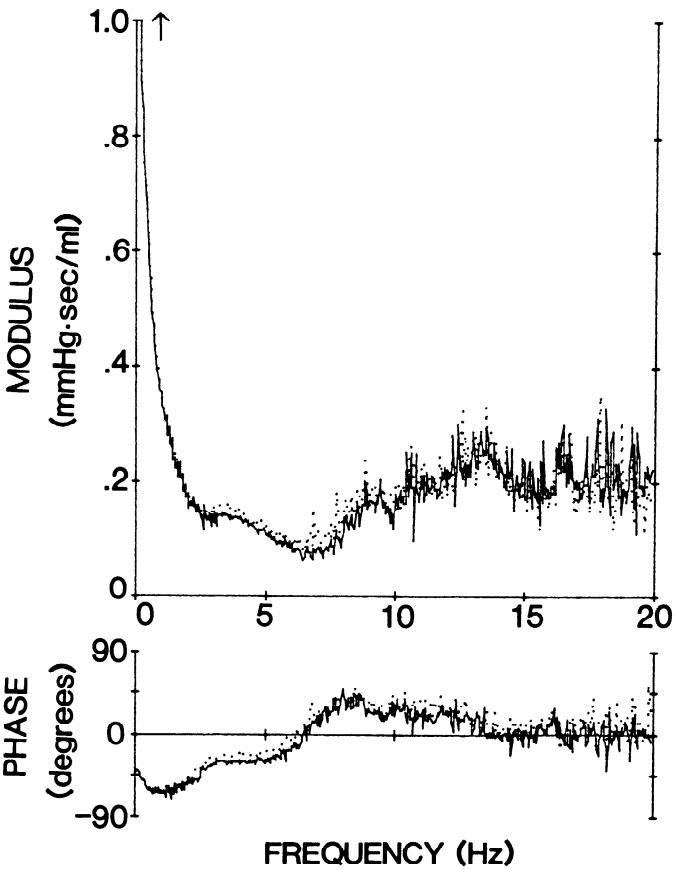

FIG. 9. Validation of simulation. Experimentally determined impedance modulus (*top*) and phase (*bottom*) are shown by ——. This impedance was imposed on model ventricle using mathematical techniques detailed in APPENDIX 1. We simulated random pacing of model ventricle, stored aortic pressure and flow data, and redetermined impedance, which model ventricle actually confronted. Redetermined impedance is shown by · · · · · . As shown, the 2 impedances are very close to each other, thus validating our techniques of determining impulse response and executing convolution.

modified impedance spectrum, $Z'(\omega)$. There is one consideration, however, that necessitates some supplementation of the measured impedance data. Because we use a computer to accomplish computations, all time signals [e.g., AoF(t), $\alpha(t)$, and $z'(t)$] are stored as discrete time sequences rather than truly continuous signals. The digitization time interval between points of the impulse response (Δt) is determined by the reciprocal of the maximum frequency of the aortic input impedance spectrum (Hz_{max})

$$\Delta t = 1/Hz_{max} \qquad (A14)$$

As described in METHODS, we could measure the impedance spectrum up to a maximum frequency of ~20 Hz; this would result in an impulse response with a Δt of 50 ms. However, for simulating the coupling between ventricle and arterial system, 50-ms step sizes are much too large. Empirical observations indicated that a Δt of 10 ms is reasonable, therefore requiring that the impedance spectrum be known up to 100 Hz. To accomplish this, we assumed that the modulus of the impedance at frequencies higher than the measured Hz_{max} was equal to the characteristic impedance and that the phase decayed to 0°. These assumptions seem justified by consideration of the fact that this is similar to the behavior of the Windkessel model at high frequencies. After this padding procedure, $z'(t)$ was calculated by inverse Fourier transformation using a Radix-2 FFT algorithm. To use the Radix-2 FFT algorithm it is required that the number of discrete points in the aortic impedance spectrum be equal to an integer power of 2; our spectra, now extended to 100 Hz, were composed of a total of 1,024 points (2^{10} points). The duration of the resulting impulse response was 10.24 s (1,024 points × 10 ms/point = 10.24 s).

APPENDIX 2

Verification of mathematical techniques. In view of the large amount of data manipulation required to generate the impulse response and to execute its coupling to the model ventricle, one may wonder whether we were really imposing the desired impedance in our computer simulation. To verify that we were, we imparted onto our model ventricle a realistic force-interval relationship [i.e., the contractility on a given beat was dependent on the history of the interval between beats (2, 29)] and then programmed the simulation so that the interval between beats was random. The afterload was the impulse response of an experimentally determined impedance spectrum. We stored the resulting AoP and AoF data for 4 min of simulated real time, then determined the impedance spectrum as we had done for the real data. The result of this procedure for one spectrum is presented in Fig. 9. The solid line represents the original experimentally determined impedance spectrum and the dotted line represents the redetermined spectrum from the computer simulation data. The DC resistance value was 2.87 mmHg·s·ml^{-1} for the original and 2.86 mmHg·s·ml^{-1} for the redetermined spectra. As shown, the simulated afterload impedance very closely matches the measured impedance in all its details. The only significant difference was noted in the phase data where there was a very slight upward shift of the simulated impedance that was <10°, most prominent at frequencies between 1 and 7 Hz. Despite this, the frequency at which the phase crossed the horizontal axis was not significantly influenced nor was the phase at higher frequencies.

The authors are grateful to Dr. K. Sagawa for encouragement, support, and valuable advice throughout this investigation and preparation of the manuscript. We also thank Dr. William C. Hunter for valuable discussions and advice during this study.

Support for this research was provided by National Heart, Lung, and Blood Institute Grant HL-14903.

Address for reprint requests: D. Burkhoff, Traylor Building, Rm. 223, Dept. of Biomedical Engineering, the Johns Hopkins Medical School, 720 Rutland Ave., Baltimore, MD 21205.

Received 11 May 1987; accepted in final form 16 May 1988.

REFERENCES

1. BURKHOFF D., AND K. SAGAWA. Ventricular efficiency predicted by an analytical model. *Am. J. Physiol.* 250 (*Regulatory Integrative Comp. Physiol.* 19): R1021–R1027, 1986.
2. BURKHOFF, D., D. T. YUE, M. R. FRANZ, W. C. HUNTER, AND K. SAGAWA. Mechanical restitution of isolated perfused canine left ventricles. *Am. J. Physiol.* 246 (*Heart Circ. Physiol.* 15): H8–H16, 1984.
3. CAMPBELL, K. B., J. A. RINGO, AND J. E. ALEXANDER. Informational analysis of left-ventricle/systemic-arterial interaction. *Ann. Biomed. Eng.* 12: 209–231, 1984.
4. ELZINGA, G., AND M. WESTERHOF. Pressure and flow generated by the left ventricle against different impedances. *Circ. Res.* 32: 178–186, 1973.
5. HUNTER, W. C., J. S. JANICKI, K. T. WEBER, AND A. NOORDERGRAFF. Flow-pulse response: a new method for characterization of ventricular mechanics. *Am. J. Physiol.* 237 (*Heart Circ. Physiol.* 6): H282–H292, 1979.
6. KENNER, T. Models of the arterial system. In: *The Arterial System*, edited by R. D. Bauer and R. Busse. Berlin: Springer-Verlag, 1978, p. 80–88.
7. LATSON, T. W., W. C. HUNTER, D. BURKHOFF, AND K. SAGAWA. Time sequential prediction of ventricular-vascular interactions. *Am. J. Physiol.* 251 (*Heart Circ. Physiol.* 20): H1341–H1353, 1986.
8. LAXMINARAYAN, S., P. SIPKEMA, AND N. WESTERHOF. Characterization of the arterial system in the time domain. *IEEE Trans. Biomed. Eng.* 25: 177–184, 1978.
9. MILNOR, W. R. Arterial impedance as ventricular afterload. *Circ. Res.* 36: 565–570, 1975.
10. MURGO, J. P., N. WESTERHOF, J. P. GIOLMA, AND S. A. ALTOBELLI. Aortic input impedance in normal man: relationship to pressure wave shape. *Circulation* 62: 105–116, 1980.
11. NICHOLS, W. W., M. F. O'ROURKE, A. P. AVOLIO, T. YAGINUMA, J. P. MURGO, C. J. PEPINE, AND R. CONTI. Effects of age on ventricular-vascular coupling. *Am. J. Cardiol* 55: 1179–1184, 1985.
12. NOBEL, M. I. M. Left ventricular load, arterial impedance and their interrelationship. *Cardiovasc. Res.* 13: 183–198, 1979.
13. O'ROURKE, M. F. Arterial hemodynamics in hypertension. *Circ. Res.* 26, *Suppl.* 2: 123–133, 1970.
14. O'ROURKE, M. F. *Arterial Function in Health and Disease.* Edinburgh: Churchill Livingston, 1982.
15. PEPINE, C. J., W. W. NICHOLS, AND C. R. CONTI. Aortic input impedance in heart failure. *Circulation* 58: 460–465, 1978.
16. PIENE, H. Interaction between the right ventricle and its arterial load: a quantitative solution. *Am. J. Physiol.* 238 (*Heart Circ. Physiol.* 7): H932–H937, 1980.
17. SHROFF, S. G., J. S. JANICKI, AND K. T. WEBER. Evidence and quantitation of left ventricular systolic resistance. *Am. J. Physiol.* 249 (*Heart Circ. Physiol.* 18): H358–H370, 1985.
18. SIPKEMA, P., N. WESTERHOF, AND O. S. RANDALL. The arterial system characterized in the time domain. *Cardiovasc. Res.* 14: 270–279, 1980.
19. SUGA, H., R. HISANO, Y. GOTO, O. UAMADA, AND Y. IGARASHI. Effect of positive inotropic agents on the relation between oxygen consumption and systolic pressure volume area in canine left ventricle. *Circ. Res.* 53: 306–318, 1983.
20. SUGA, H., AND K. SAGAWA. Instantaneous pressure-volume relationship and their ratio in the excised, supported canine left ventricle. *Circ. Res.* 35: 117–126, 1974.
21. SUNAGAWA, K., D. BURKHOFF, K. O. LIM, AND K. SAGAWA. Impedance loading servo pump system for excised canine ventricle. *Am. J. Physiol.* 243 (*Heart Circ. Physiol.* 12): H346–H350, 1982.
22. SUNAGAWA, K., W. L. MAUGHAN, AND K. SAGAWA. Optimal arterial resistance for the maximal stroke work studied in isolated canine left ventricle. *Circ. Res.* 56: 586–595, 1985.
23. SUNAGAWA, K., W. L. MAUGHAN, D. BURKHOFF, AND K. SAGAWA. Left ventricular interaction with arterial load studied in isolated canine ventricle. *Am. J. Physiol.* 245 (*Heart Circ. Physiol.* 14):

H773–H780, 1983.
24. TAYLOR, M. G. Use of random excitation and spectral analysis in the study of parameters of the cardiovascular system. *Circ. Res.* 18: 585–595, 1966.
25. WESTERHOF, N., F. BOSMAN, C. J. DE VRIES, AND A. NOORDERGRAAF. Analog studies of the human systemic arterial tree. *J. Biomech.* 2: 121–143, 1969.
26. WESTERHOF, N., G. ELZINGA, AND P. SIPKEMA. An artificial arterial system for pumping hearts. *J. Appl. Physiol.* 31: 776–781, 1971.
27. YIN, F. C. P. *Ventricular/Vascular Coupling.* New York: Springer-Verlag, 1987.
28. YIN, F. C. P., Z. LIU, AND K. P. BRIN. Estimation of arterial compliance. In: *Ventricular/Vascular Coupling,* edited by F. C. P. Yin. New York: Springer-Verlag, 1987, p. 384–398.
29. YUE, D. T., D. BURKHOFF, M. R. FRANZ, W. C. HUNTER, AND K. SAGAWA. Postextrasystolic potentiation of the isolated canine ventricle: relationship to mechanical restitution. *Circ. Res.* 56: 340–350, 1985.